ELSEVIER

Surface Science 345 (1996) 41–52

surface science

The growth of silver on a ruthenium($10\bar{1}0$) surface

Petra Lenz-Solomun [b], K. Christmann [a,*]

[a] *Institut für Physikalische und Theoretische Chemie, Freie Universität Berlin, D-14195 Berlin, Germany*
[b] *Institut für Experimentalphysik der Freien Universität Berlin, D-14195 Berlin, Germany*

Received 13 February 1995; accepted for publication 15 August 1995

Abstract

The interaction of Ag with a Ru($10\bar{1}0$) surface has been examined between 80 and 500 K using LEED, AES, TPD and chemisorptive titration techniques. Interestingly, we observe a stable Ag-induced c(2×2) LEED phase over the large coverage (Θ) range ($0.06 \leqslant \Theta \leqslant 0.65$), indicating the formation of two-dimensional ordered Ag islands due to attractive Ag–Ag interactions. As Θ reaches ~0.6, further Ag deposition causes parallel first-layer filling and gradual 3D-clustering, accompanied by the successive development of (incomplete) (10×1) and c(14×5) structures. This latter phase remains stable up to the largest silver coverages studied ($\sim\Theta\approx 6$–8). Titration with CO and/or hydrogen reveals that even for $\Theta = 5$ a few Ru sites remain accessible pointing to a somewhat porous Ag overlayer. In TPD, two binding states appear which we associate with chemisorbed and condensed Ag, respectively, whereby the first state exhibits an increase of the binding energy at medium Θ due to attractive interactions, and the second (multilayer state) corresponds to the sublimation enthalpy of bulk silver. Our combined results indicate a simultaneous multilayer (SM) or a pseudo-Frank–van-der-Merwe growth leading to relatively rough Ag films whose structure is determined by the corrugation of the Ru substrate: true epitactic growth of Ag cannot be observed up to 8 nominal Ag monolayers.

Keywords: Auger electron spectroscopy; Epitaxy; Low energy electron diffraction (LEED); Thin film growth

1. Introduction

The growth, morphology and physical properties of thin metal films deposited onto metal substrates of a different kind (often termed "heteroepitaxy") have attracted a considerable interest from both fundamental and applied physical viewpoints. Thin metal films may grow either *pseudomorphically*, with the lattice parameters forced by the structure of the substrate, or with their own characteristic lattice constants, whereby only the orientation and direction of growth is influenced by the substrate. For more details, we refer to the fundamental considerations by Bauer [1–3]. Surface physicists are interested in the energetics, kinetics, and type of growth and their correlation with macroscopic thermodynamic properties, such as the surface tensions of the two materials. In applied physical chemistry, among others the *catalytic* properties of thin metallic films deserve great attention, in particular with respect to correlations between activity and film dispersion and/or thickness. Chemical additives can also dramatically modify both the catalytic activity and selectivity, whereby multicomponent thin films can easily be prepared by simultaneous deposition in vacuo. Accordingly, many adsorption and reaction studies have been concerned with thin metal films [4]. We recall that binary alloy or bimetallic catalyst materials are frequently used in practical heterogeneous cataly-

* Corresponding author. Fax: +49 30 838 6612.

SSDI 0039-6028(95)00870-5

sis, and numerous studies reported in the literature [5–8] focused on their preparation and characterization under UHV conditions:

Adsorption and catalysis studies on bimetallic materials by Houston et al. [9], Rodriguez et al. [10], Sachtler and Somorjai [11,12], Campbell et al. [13], Paffett et al. [14], Koel et al. [15], Peebles et al. [16], Paul and Hoffmann [17], Hoffmann and Paul [18] as well as in our own laboratory [19–21] have contributed to a better understanding of the chemical action of the (metallic) additive to a metal single crystal surface. A revealing result was, among others, that dissociative adsorption (H_2, N_2, O_2) is often hampered by the requirement of two or more adjacent adsorption sites. Consequently, a pronounced ensemble-effect can govern the adsorption and surface binding even of a simple diatomic species. The lateral distribution of the additive's atoms is therefore crucial and calls for studies of the dispersion and growth of the deposit, whereby it is advantageous, when it does not form alloys with the underlying substrate, which in turn rules out segregation or depletion effects in the surface region. Alloying usually does not take place for noble metal deposition on refractory metal surfaces, the adsorption of Cu, Ag, Au on W and Mo surfaces being a good example [22–25].

There exists also a number of studies dealing with the growth of Cu, Ag, and Au on Ru surfaces, whereby mostly the basal (0001) plane was used as a host substrate for the thin film growth: Cu on Ru(0001) was extensively studied by Yates et al. [26], Goodman and Peden [27] and Peden and Goodman [28], by Brown and Vickerman [29] and in our own laboratory [30,31]. The adsorption of Ag on Ru(0001) was investigated by Wandelt et al. [32] and Niemantsverdriet et al. [33], and Au on Ru(0001) was studied by Harendt et al. [34] by combined LEED, AES, and TPD measurements, and more recently by Hwang et al. [35,36] and Pötschke et al. [37] by means of scanning tunneling microscopy (STM). These latter studies are particularly revealing as STM could nicely image the various stages of Au film growth on the Ru surface. The main result was that the formation of (strongly dendritic) two-dimensional islands prevails in the submonolayer concentration regime, followed by the formation of one or two (incomplete) Au monolayers and subsequent three-dimensional clustering, if the deposition is performed at and below 300 K. Higher deposition temperatures generally favor layer-by-layer growth, with the degree of two-dimensional order depending on the deposition conditions.

In view of the open crystallography and the chemical activity of the hcp. $(10\bar{1}0)$ surface we found it interesting to study the growth of thin silver films on the Ru$(10\bar{1}0)$ surface which was not so often used for noble metal deposition. In this respect, we mention our own investigation of the adsorption of gold onto the Ru$(10\bar{1}0)$ surface [38], as well as a very recent study by Poulston et al. [39] on the same system.

Here, we report on combined low-energy electron diffraction (LEED), Auger electron spectroscopy (AES), temperature-programmed thermal desorption (TPD), and gas-adsorption–titration measurements to characterize the adsorption and growth of silver films on the Ru$(10\bar{1}0)$ surface; an account of the adsorptive and catalytical properties of this bimetallic system has been given elsewhere [40].

2. Experimental

2.1. Experimental setup

The experiments were performed in an ion-getter pumped ultra-high vacuum (UHV) chamber described previously [41]. The apparatus was equipped with a four-grid LEED optics, a cylindrical mirror analyzer (CMA) for AES, a quadrupole mass filter for TPD, and a Kelvin probe for recording work function changes. A base pressure of 10^{-10} mbar was routinely obtained; during the operation of the vapor source (see below) the pressure remained in the low 10^{-10} mbar range. Ultrapure gases (CO, H_2) were used in the chemisorptive titration experiments and admitted to the chamber via bakeable stainless-steel leak valves. The Ru sample was oriented by means of Laue X-ray diffraction and cut by spark erosion; it was mechanically and electrochemically (NaClO solu-

tion) polished and cleaned in the usual manner (cf. Ref. [33]), before it was mounted to a sample manipulator which allowed in situ positioning as well as heating ($T_{max} \approx 1800$ K) and cooling (via liquid N_2) ($T_{min} \approx 90$ K). The Ru temperature was measured using a Ni/CrNi thermocouple spot-welded to the rear of the crystal; the signal was fed to a special temperature regulator designed by Conrad et al. [42]. The main cleaning procedure of the Ru sample consisted in heating in oxygen ($P_{O_2} \approx 10^{-7}$ mbar), followed by a short heating to 1500 K in order to remove residual oxygen. The final cleaning was achieved by gentle argon ion sputtering and subsequent annealing at 1400 K. The surface cleanliness was judged from (i) the quality of the (1×1) LEED pattern (bright and sharp diffraction spots on a low background), (ii) the shape and intensity ratios of the AES signals [43,44], and (iii) (most sensitively) from the total work function increase ($\Delta\Phi \approx 420$ meV) caused by a saturation coverage of hydrogen [45].

2.2. The deposition of silver; coverage calibration

The silver deposits were obtained from a DC operated and power-controlled thermal effusion cell which was loaded with ultrapure (5 N) Ag wire. After appropriate outgassing of the source the as-deposited Ag films were very clean; they usually neither showed carbon nor sulfur contaminations and did not need further sputter-cleaning. Although we could not calibrate our source *quantitatively* we could establish, from combined LEED and TPD observations described in more detail later, approximate deposition rates ranging from a few Ag monolayers per hour to several layers per minute. An important control parameter is the silver coverage Θ, which we define (as usual) as the total number of Ag atoms adsorbed on top of the Ru surface divided by the number of topmost Ru surface atoms ($=8.67 \times 10^{18}$ m^{-2} for the (10$\bar{1}$0) orientation). In a certain coverage range the Ag atoms form a c(2×2) phase, whereby structural considerations presented in Section 4 suggest that three Ag atoms are adsorbed on top of four Ru surface atoms resulting in $\Theta = 0.75$ for the c(2×2) phase. At the c(2×2) LEED intensity maximum all Ag atoms can be desorbed and a representative fraction collected by means of a mass spectrometer, and the area under the resulting TPD curve $\int P_{Ag}\, dt$ can serve as a calibration point for $\Theta = 0.75$. The only requirement is that the Ru surface is uniformly covered with the homogeneous c(2×2) phase. Hence, by comparison with our "c(2×2)TD spectrum" all other Ag TPD curves can be converted to the absolute Θ scale. Note that the term *coverage* defined above refers, in the first instance, to a two-dimensional layer. However, as will be shown below, there occurs some three-dimensional clustering, before the Ru surface becomes uniformly coated with the c(2×2) phase. At the c(2×2) LEED intensity maximum about 4/5 of the Ru surface is actually covered by this phase; the "open" Ru area is only gradually covered as the Ag deposition continues, while at the same time Ag atoms reside already in the second and/or third Ag layer and, strictly speaking, do not contribute to the coverage in the above sense. One could define a coverage for every layer, i.e., $^1\Theta$ for the first, $^2\Theta$ for the second and $^3\Theta$ for the third layer etc., and the respective *layer-specific* coverage is, in principle, available from the shape of the TPD spectra with their individual state-related peaks (β_2 and β_1 in our case), a requirement being a sufficiently large difference in the states' binding energy. Clearly, the β_2 state is associated with the first-layer coverage $^1\Theta$. The limited resolution of our TD experiment along with vanishing differences in the binding energies of the second, third etc. Ag layers does not allow a distinction between $^2\Theta$, $^3\Theta$, $^4\Theta$ etc. Furthermore, in order to delineate between $^1\Theta$ and $\Sigma_{i=2}^{\infty} \Theta_i$ any interlayer equilibration *during* the heating would change the Θ_i values. Equilibration between β_2 and β_1 could be ruled out by a series of experiments, in which such amounts of Ag were deposited which led to an incomplete filling of both the β_2 and the β_1 state, followed by thermal desorption with different heating rates ranging between $0.1\ \mathrm{K\ s^{-1}} < \mathrm{d}T/\mathrm{d}t < 20\ \mathrm{K\ s^{-1}}$: the relative fractions of β_1 and β_2 were independent of the heating rate.

For most of the following considerations it is sufficient to know just the (*non*-layer-specific) overall amount of Ag deposited onto the Ru surface which we denote as *nominal* coverage $\Theta = \Sigma_{i=2}^{\infty} \Theta_i$.

This means for example, that $\Theta = 1.2$ is equal to a total amount of silver which is 1.2 times the monolayer coverage ${}^1\Theta$, i.e. $1.2 \times 8.638 \times 10^{18}\ m^{-2} = 1.04 \times 10^{19}\ m^{-2}$, regardless of its distribution between the various layers. It also follows that as long as the deposited Ag atoms reside only in the first layer, the nominal coverage Θ is identical with ${}^1\Theta$.

3. Results

3.1. Low-energy electron diffraction (LEED)

The clean, well-annealed Ru(10$\bar{1}$0) surface exhibits a LEED pattern with bright and very sharp diffraction spots on a low background indicating a chemically clean and crystallographically well-ordered substrate surface. After this characterization the deposition of Ag was performed with the substrate temperature kept fixed; although we deposited some Ag films also at temperatures around 80 K (see further below), most of the deposition experiments were carried out with the Ru sample kept at $T \approx 735$ K in order to give the deposited Ag atoms sufficient mobility to reach the energetically most favorable adsorption sites.

Even quite small Ag surface concentrations (beginning at $\Theta \approx 0.08$) result in the formation of distinct LEED spots of a c(2×2) pattern, from which we reproduce a photograph in Fig. 1a. As we continue the Ag deposition, the fractional-order beams of the c(2×2) pattern gradually increase in intensity until they reach a flat maximum and drop fairly sharply as Θ approaches 0.6. The respective coverage dependence of the c(2×2) pattern is reproduced in Fig. 2, with the fractional-order beam intensity (measured by our video LEED system) being plotted as a function of the *relative* Ag coverage (which follows directly from the β_2 silver TPD peak area, cf. Section 3.2). Most remarkable is the wide coverage range in which the c(2×2) structure exists: the respective pattern can be observed for $0.08 < \Theta < 0.65$. The formation of the c(2×2) structure indicates a significant mutual Ag–Ag interaction which we believe is predominantly of attractive character, since our TPD and AES results suggest a formation of islands within the first layer. Possible real-space structure models for the c(2×2) phase will be discussed in Section 4.1.1.

Shortly before the c(2×2) intensity disappears around $\Theta \approx 0.65$ we can observe spots of a (10×1) LEED structure which indicates that the c(2×2) is followed by a second Ag phase with long-range order. Its LEED pattern is reproduced in Fig. 1b; as can be seen from this figure only the first and at most also the second-order superstructure beams appear, the reasons likely being poor long-range periodicity and systematic extinctions due to phase relations inside the unit-cell (which we have, however, not systematically analyzed). Between $0.6 < \Theta < 0.85$ there is a coexistence range of the c(2×2) and a subsequent (10×1) phase (this situation is actually depicted in Fig. 1b). We note that both structures clearly appear within the monolayer coverage range. There follows a fairly narrow coverage range ($0.85 < \Theta < 0.95$) in which *only* the (10×1) phase is visible. As Θ increases beyond 0.95, there follows a fairly complex LEED pattern which we denote as c(14×5) structure. However, quite similar to the preceding (10×1) pattern only the first and second-order diffraction maxima are visible, for the same reasons pointed out above. We also note that the c(14×5) LEED structure coexists over a narrow coverage range ($0.95 < \Theta < 1.1$) with the (10×1) phase. The c(14×5) phase represents the final LEED structure; once the (10×1) pattern has disappeared around $\Theta = 1.1$ this phase is *exclusively* visible and persists up to the largest coverages investigated in our study, i.e. $\Theta \approx 6 \cdots 8$. It is therefore very likely that the c(14×5) is associated with the multilayer Ag phase. The LEED pattern of the (incomplete) c(14×5) structure is reproduced in Fig. 1c. Silver coverages beyond two or three monolayers do not improve the long-range order of the c(14×5) phase but only add background to the pattern indicating the buildup of further, poorly ordered Ag layers. We remark that throughout our Ag deposition/annealing experiments it was never possible to observe the formation of an Ag-induced (1×1) phase which rules out a pseudomorphical growth of Ag in the monolayer coverage range.

If we lower the deposition temperature to 375 K there are no principal changes. Rather, the LEED

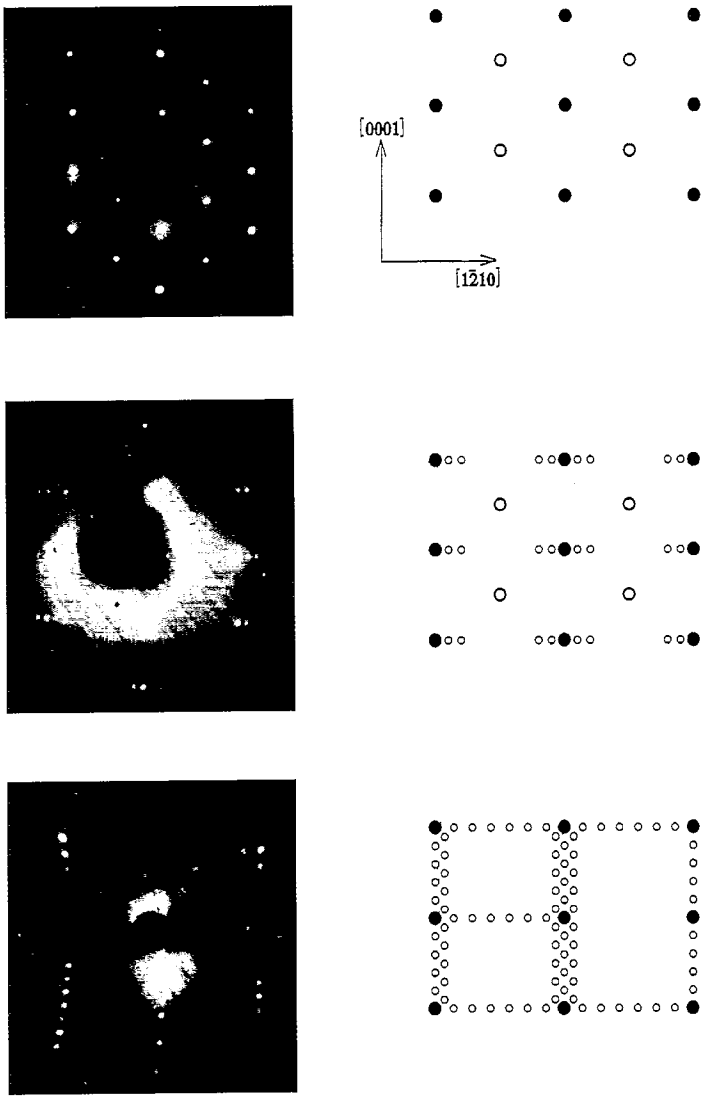

Fig. 1. LEED patterns observed with silver on a Ru(10$\bar{1}$0) surface at a deposition temperature of 735 K; photographs shown on the left, schematical drawings on the right. (a) c(2 × 2) pattern at the respective LEED intensity maximum ($\Theta \approx 0.6$); (b) superposition of the c(2 × 2) structure with the (10 × 1) pattern ($\Theta \approx 0.75$). Most of the fractional higher-order beams are not visible, only those which are close to a substrate LEED spot appear with appreciable intensity due to the non-primitive structure of the unit mesh and poor long-range order. (c) c(14 × 5) structure at a Ag coverage of $\Theta \geqslant 1.2$; again, as with the (10 × 1) structure, most of the "extra" spots remain invisible.

features become somewhat diffuse, the spots are not as bright, but the superstructures appear practically within the same Ag coverage ranges. However, at the lowest deposition temperature studies, namely $T = 80$ K, we only obtain a very blurred and diffuse c(2 × 2) pattern, while the (10 × 1) phase is not visible anymore. The c(14 × 5), if observable at all, always contains a large diffuse background contribution under these conditions pointing to a fair amount of disorder.

3.2. Temperature-programmed thermal desorption (TPD)

A series of silver thermal desorption spectra after Ag deposition at $T > 375$ K is reproduced in Fig. 3.

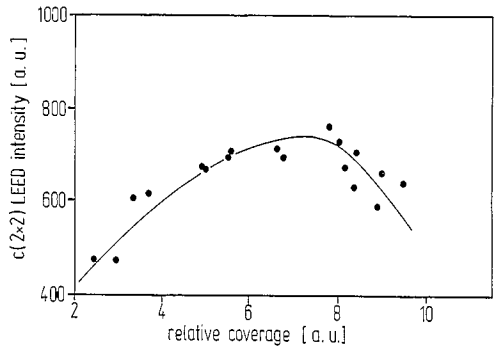

Fig. 2. Dependence of the c(2 × 2) Ag long-range order on the silver coverage. The fractional-order LEED beam intensity is plotted against the Ag coverage Θ, with Θ being determined from a correlation of the thermal desorption curves with the real-space structure model shown in Fig. 7.

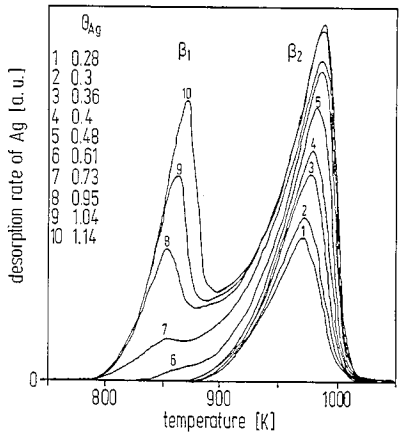

Fig. 3. Series of silver thermal desorption spectra (amu 108), obtained from Ru surfaces covered with increasing amounts of Ag at $T \approx 735$ K. Clearly, two desorption states β_2 and β_1 can be distinguished which develop with increasing coverage. We associate the β_2 state with Ag atoms of the first layer and the β_1 state with Ag multilayers.

Two desorption states can be distinguished, viz., a single maximum between 970 and 990 K at small coverages which we assign as β_2 state. With increasing Θ this maximum shifts somewhat to higher temperatures. This behavior reflects a fractional-order desorption kinetics and/or the operation of attractive Ag–Ag interactions (which are responsible for the existence of the c(2 × 2) structure in the submonolayer coverage range). A fractional-order kinetics usually indicates preferential desorption of particles from the perimeters of islands. In accordance with many previous investigations [19,32,34] we identify the β_2 state as the desorptive contribution from deposit atoms having direct contact with the Ru surface. At a coverage of $\Theta \approx 0.6$ a second state (denoted as β_1) grows in as a shoulder on the low-temperature tail of the β_2 state; its maximum can be located between 850 and 880 K, depending on the coverage. A consistent interpretation is that β_1 reflects the Ag atoms from the second layer (and all further layers). Accordingly, this state grows strongly as we increase the coverage and finally dominates (around $\Theta \geqslant 3$), the entire TPD spectrum and then also exhibits a reaction-order close to zero as expected for a sublimation process. Interestingly, there is, in a certain coverage interval, a *simultaneous* growth of both β_1 and β_2 desorption states. This indicates that the second Ag monolayer begins to grow before the first layer is really completed.

We have subjected the thermal desorption states to a line-shape analysis proposed by King [46] and obtained the (Θ-dependent) activation energies for desorption, E^*_{des}, shown in Fig. 4. This procedure works well for individual or sufficiently separated desorption states and has been successfully applied several times in the past [30–34]. We find an initial *increase* of the desorption energy from 255 (±20) kJ/mol up to a maximum of ~305 (±10) kJ/mol around $\Theta \approx 0.4$ as the β_2 state becomes increasingly populated. Thereafter E^*_{des} drops again until it reaches, for $\Theta \approx 0.6$, where the

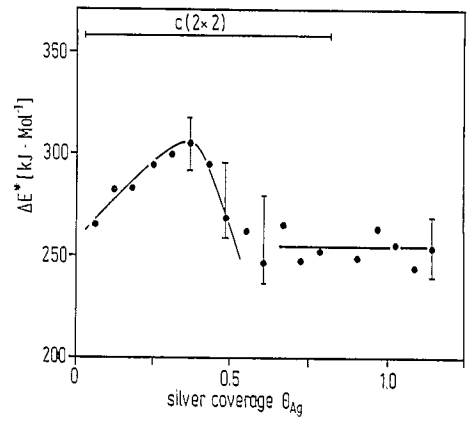

Fig. 4. Activation energies of desorption ΔE^* as a function of the Ag surface coverage as determined by a line-shape analysis after King [46]. The maximum approximately coincides with the LEED intensity maximum of the c(2 × 2) phase.

β_1 state starts to become filled, a value 260 (± 10) kJ/mole, at which level it apparently remains for all higher coverages studied ($\Theta \approx 8$). As the *simultaneous* filling of β_2 and β_1 between $0.6 < \Theta < 1.1$ represents a metastable situation, the E^*_{des} values come out too low in this coverage range; therefore, our data reflect at best a kind of a lower limit for the activation energies here as indicated by the asymmetric error bars of Fig. 4.

3.3. Auger electron spectroscopy (AES)

We have taken Auger electron spectra of the clean and the Ag-covered Ru(10$\bar{1}$0) surface after deposition at $T = 745$ K. In order to quantify the deposited amounts of Ag, we determined the intensities of the Ru $M_5N_3N_5$ transition at 231 eV and of the Ag $M_5N_{4.5}N_{4.5}$ transition at 356 eV. A plot of the Auger signal intensities versus the Ag coverage as determined from our TPD data is shown in Fig. 5. For both the Ru and Ag AES intensity we can distinguish two linear sections, viz., a first one for $0 < \Theta < 0.75$, and a second one for $0.75 < \Theta < 1.6$, whereby the second section has a somewhat reduced slope. Due to the relatively large scatter of the data points it is impossible to delineate further linear sections at higher Ag coverages.

The occurrence of distinct breaks in an Auger intensity versus coverage plot usually indicates a layer-by-layer growth mode (Frank–van-der-Merwe mechanism) [47]. If this kind of growth mode prevails in the entire coverage range (including the multilayer regime) one would expect that the Auger signal intensity of the Ru substrate should have decayed to zero once the escape depth of the respective 230 eV electrons is shorter than the average film thickness (this escape depth can be estimated from values given in the literature for a related quantity, the inelastic mean free path λ_{imfp} [48,49], to range between 10 and 20 Å, which is just in the range of a 5 monolayer thick Ag film). However, even after the deposition of five nominal Ag monolayers the Ru Auger lines can be quite clearly observed, and also from our gas chemisorption titration measurements it seems as if at least a few Ru adsorption sites remain uncovered by Ag atoms under these conditions. The AES results of Fig. 5 can therefore be reconciled with a silver growth in which the first two monolayers remain somewhat incomplete and the subsequent layers exhibit three-dimensional clusters and islands rather than a perfect layering. Taking the TPD and AES results together and also considering the titration experiments of Section 3.4 below, we may conclude on an imperfect layer growth [50,51].

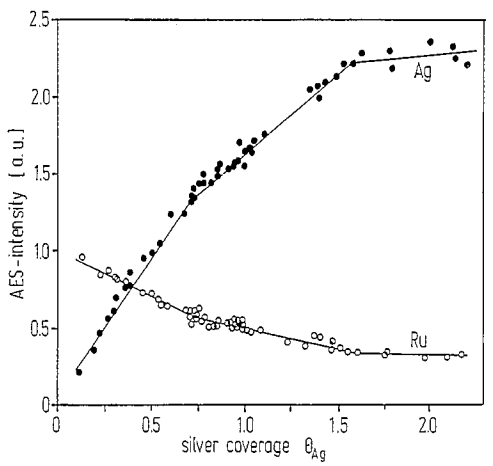

Fig. 5. Plot of the Auger signal intensities versus the Ag coverage. For both Ru and Ag the AES signal intensity versus Ag coverage plot exhibits two breaks which may be associated with the formation (of a still some what incomplete) Ag monolayer.

3.4. Chemisorptive titration with carbon monoxide CO and hydrogen H_2

Because the main body of our CO adsorption and CO+hydrogen co-adsorption results have been published in detail elsewhere [40], we can keep the respective presentation quite short and focus on some titration data which corroborate the aforementioned assumptions about the silver growth mode. We subjected the Ag/Ru surfaces to exposures of more than 10 L of CO at 300 K and performed CO TPD experiments. A typical result is shown in Fig. 6, where the CO TD peak integral is plotted against the nominal silver coverage Θ. From previous CO adsorption studies with bimetallic Cu, Ag, and Au/Ru surfaces it has become apparent [20,21,40] that (i) CO does not adsorb on the noble metal atoms at room temperature and that (ii) the CO molecule requires less than two adjacent Ru atoms to become strongly

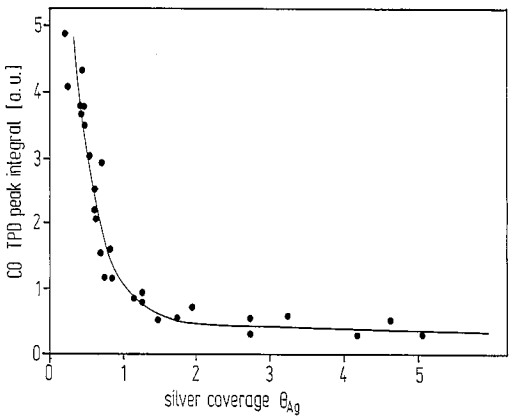

Fig. 6. Plot of the CO thermal desorption peak intensity (amu 28) against the nominal silver coverage; CO was exposed to the bimetallic surface at room temperature.

adsorbed. We therefore tend to interpret the continuous CO adsorption even after deposition of 5 nominal Ag monolayer as evidence of the existence of some scattered "pores" in the silver film where CO molecules can still get into adsorptive contact with Ru surface.

Principally similar results were obtained from our hydrogen titration studies, although the hydrogen uptake decays to zero already around $\Theta \approx 5$, probably due to the operation of a pronounced ensemble effect which is involved in the dissociation of the H_2 molecules [19,21].

4. Discussion

4.1. Structure models for the LEED phases

4.1.1. The c(2 × 2) phase

The correct determination of the Ag coverage is tied to a realistic real-space structure model for the c(2 × 2) phase. Excluding a Ag-induced surface reconstruction of the Ru substrate (for which we do not have any hint) we may clearly attribute this superstructure to a long-range order within the Ag deposit. In principle, a c(2 × 2) structure which occurs in the submonolayer range can reflect absolute coverages of 0.5 (with a *primitive* centered unit mesh containing just a single centered adsorbate atom) or 0.75 (with a non-primitive unit mesh containing two off-centered adsorbate atoms). From the combined LEED, TPD and AES measurements we obtained the information that the LEED intensity maximum of the c(2 × 2) roughly coincides with (i) the beginning growth of the β_1 TPD state and (ii) the first break in the Auger intensity/Ag surface concentration plot. This would justify to associate the c(2 × 2) structure with the monolayer coverage. Two observations contradict this interpretation: (i) the β_2 state (which we believe is caused by the Ag atoms in direct contact with Ru) is not yet saturated at this point, but filled only to about 70%, and (ii) shortly after the c(2 × 2) intensity maximum and still in the range where the β_2 state increases the transient (10 × 1) structure appears. Therefore, also this phase reflects a coverage $\Theta \leqslant 1$ monolayer; as will be shown below, we associate it with $\Theta = 0.9$. The TPD peak areas of the c(2 × 2) and the (10 × 1) are related by a factor of 0.8 (and not 0.6) which rules out a *primitive* c(2 × 2) unit mesh with $\Theta = 0.5$ and supports a *non-primitive* unit mesh with $\Theta = 0.75$. In Fig. 7 we present a respective real-space structure model of the c(2 × 2) in which two non-equivalent adsorption sites are occupied, viz., atop and bridge sites. In our model we have arbitrarily chosen the Ru rows providing the bridge sites and the Ru troughs providing the atop sites, but we could change this assignment with equal justification, since our experiments do not allow a distinction. Note that the metallic radius of a silver atom is 1.44 Å, while that of a Ru atom is 1.35 Å [52], which means that the Ag atoms are by ~6% larger than the Ru atoms. In the structure model of Fig. 7 the Ag atoms have a nearest-neighbor distance of ~6.9 Å and are, hence, only loosely packed, the reason being that the Ru(10$\bar{1}$0) surface exhibits an "open" crystallography. However, due to the inhomogeneity of the adsorption sites a *corrugated* Ag layer results from our structure model, because the Ag atoms in the bridge positions on the Ru rows stick out considerably compared to the Ag atoms located in the atop sites within the troughs.

4.1.2. The (10 × 1) phase

The (10 × 1) structure following the c(2 × 2) phase is remarkably different from the foregoing structure. Obviously it is energetically more favor-

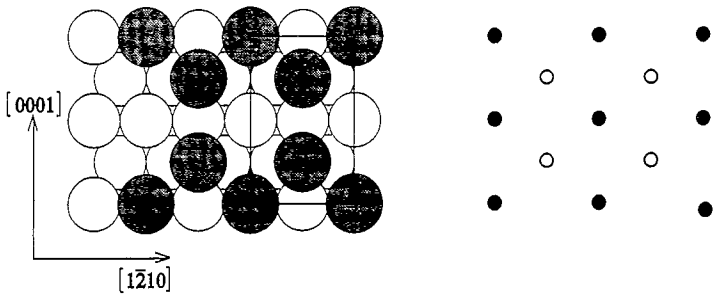

Fig. 7. Real-space structure model of the c(2×2) phase (left) corresponding to a (local) coverage of 0.75, with the unit cell being indicated. Clearly, three Ag atoms (shaded) are placed on top of four Ru surface atoms. The c(2×2) LEED pattern is shown on the right.

able not to fill the holes of the c(2×2) phase but to relax the aforementioned corrugation, and this can formally be achieved by a process in which all Ag atoms located on the Ru rows move to trough positions. Fig. 8 provides a respective structure model suggestion for the (10×1) phase. However, due to their ~6% larger radii the Ag atoms cannot really be adsorbed in equivalent sites inside the troughs, and a final situation is feasible in which a "string" of 9 Ag atoms is accommodated on top of 10 Ru trough atoms. This is depicted in the side view of Fig. 8. Of course, this is a purely tentative structure model and based on the assumption that the Ag (and Ru) atoms represent rigid balls, but it could provide a relatively simple explanation for the observed (10×1) periodicity. If we relate the number of Ag atoms to the number of Ru atoms within such a (10×1) unit cell we obtain a coverage $\Theta = 0.9$ for this structure.

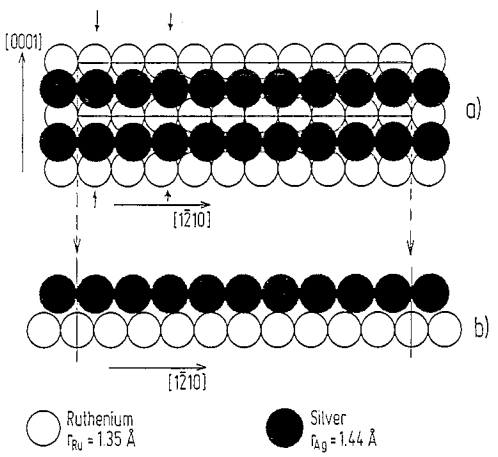

Fig. 8. (Idealized) real-space ball model of the (10×1) phase. (a) Top view showing the situation where 9 Ag atoms are accommodated on top of 10 Ru atoms; (b) side view showing the corrugation of the individual 10-atoms Ag string on top of 9 Ru trough atoms (see text for further details).

4.1.3. The c(14×5) phase

As mentioned above, the c(14×5) structure is correlated with the onset of Ag multilayer formation; a real-space structure model can easily be reconciled with densely packed Ag chains located in the furrows of the Ru(10$\bar{1}$0) surface. Because of the too large diameter of the silver atoms, the Ag atoms must be displaced not only perpendicular, but also *parallel* to the surface, that is, perpendicular to the [1$\bar{2}$10] direction across the troughs leading to a periodic distortion of the chains in [0001] direction which can be made responsible for the formation of the centered (14×5) unit mesh (which may be viewed at as an incommensurate structure), very similar to a suggestion made some years ago by Konrad et al. [53] in their study of Ag adsorption on the Ru(0001) surface. The visibility of the c(14×5) structure in a fairly large coverage range suggests that the influence of the anisotropy of the Ru(10$\bar{1}$0) surface extends up to several Ag multilayers; similar observations were previously made with the Au-on-Ru(10$\bar{1}$0) system [38,39], since the diameters of the Au and Ag atoms are very similar ($d_{Au} = 2.884$ Å [44]), and the same structural considerations hold. In their recent work on Au/Ru(10$\bar{1}$0) Poulston et al. [39] emphasize that about 15 layers of gold are necessary to overcome the structural constraints imposed by the anisotropic Ru substrate; this is completely in line with our own observations.

4.2. The binding energy and the growth mode of Ag on Ru(10$\bar{1}$0)

4.2.1. The binding energy and its coverage dependence

There exists an extensive data body of interaction energies of metallic deposits with metallic substrates and their coverage-dependences [22,30,32,34]. If we confine our discussion to noble metal–refractory (transition) metal systems and focus especially on Cu, Ag and Au interactions with Mo, W, Ru, or Re, there is a common trend in that the interaction energy becomes equal to the heat of sublimation at very large coverages, i.e., when the deposited material as a whole simply becomes vaporized from the bulk [30]. On the other hand, for the limit of very small (submonolayer) concentrations, a specific (and often coverage-dependent) "chemical" interaction between the noble metal and the substrate may show up. Typically, this energy is for noble metals only slightly larger than their heat of sublimation, due to the quite small chemical affinity (also reflected by the apparent immiscibility between noble and refractory metals). For Cu desorption from Ru(0001) we determined a difference of less than 20 kJ/mol in favor of the "chemical" interaction [30], similar to Au desorption from the same surface [34].

It is certainly justified if we assume that the desorption energy obtained for very large coverages (e.g., ~260 kJ/mol for a 20 ML thick Ag film) is practically identical with the enthalpy of sublimation of bulk Ag, which amounts to ΔH_{sub}= 266 kJ/mol [54]. Then the initial Ag–Ru interaction energy of ~255 kJ/mol (±20 kJ/mol) as determined by our line-shape analysis is of the same order of magnitude as ΔH_{sub}; it may even be a little higher. (Of course, from our error margin, also a somewhat *lower* value could be deduced, however, this would be physically unreasonable, as we should not observe two-dimensional layer growth in this case.)

Concerning the $E_{des}(\Theta)$ dependence in the submonolayer range there is a remarkable common trend, whereafter an *increase* (by some 10 kJ/mol) occurs as the coverage rises from 0 to ~half a monolayer, followed by a fall-off to about the level of the sublimation enthalpy as $\Theta = 1$ is exceeded [34]. Just this trend can be recognized in our present measurements, despite the relatively poor statistics of our data: Parallel to the formation of the c(2×2) structure, the activation energy for desorption of Ag rises by ~50 kJ/mol, and it may very well be that this rise simply reflects the (transient) attractive Ag–Ag interactions which cause the c(2×2) ordering.

Right after the c(2×2) LEED intensity maximum and parallel to the appearance of the energetically less favorable (10×1) structure, E_{des} drops by ~50 kJ/mol and reaches, after $\Theta \approx 0.75$, practically the heat of sublimation of bulk Ag. This behavior demonstrates that despite the disorder introduced by the SM growth nevertheless a silver layer is formed which resembles the Ag bulk at least with respect to the cohesive energy. On the other hand, the largely perturbed crystallography of the Ag films (at least up to a coverage of ~5 layers) shows up in the fractional-order kinetics, which points to a mechanism in which a preferential desorption from the perimeters of individual islands governs the overall rate.

4.2.2. The growth mode of Ag on Ru(10$\bar{1}$0)

Our data suggest a type of growth which is somewhere between the so-called *simultaneous multilayer* (SM) and the *incomplete* layer or pseudo-Frank–van-der-Merwe growth. The SM growth was theoretically investigated by Kashchiev [50], and experimentally verified, e.g., by Rhead et al. [51]: Due to an interplay between surface tension, cohesive energy and *kinetic* factors (diffusion coefficient, activation energy) no closed homogeneous layers can be formed. Rather, once a certain fraction of the substrate is covered by a two-dimensional film, three-dimensional aggregates grow on top of the still incomplete first layer. The *incomplete layer growth* describes a situation, where the first layers are almost complete, but as the growth continues, three-dimensional islands of the third, fourth etc. layer are formed, although the true equilibrium thermodynamics would demand the plain layer-by-layer growth. Two reasons may play a role here:

First, appreciable activation energy barriers at the edges of the two-dimensional islands may

inhibit a diffusion of the adatoms beyond these edges which effectively impairs the filling of vacancies within the layer underneath (which can only take place by a more or less "direct" impact). This limitation is usually effective at higher temperatures, where the "normal" diffusion rapidly occurs [55].

At lower temperatures, the restricted diffusivity of the deposit atoms themselves may become rate-limiting: Atoms which impinge right in the middle of an already existing first-layer island equilibrate and stick on top of the first-layer island before they can reach the energetically more favorable vacancies in the first layer, because their average diffusion length is smaller than the radius of the island. Venables [56] has recently reviewed the thermodynamical and kinetic processes involved in the crystal growth for metals on metals and metals on semiconductors.

There exist various STM investigations [35–37,57–59] which have particularly contributed to an improved insight into elementary thermodynamical and kinetic processes of homo- and heteroepitaxy, because the STM can image the morphology and shape of the nuclei and islands in real space as a function of substrate orientation, vapor flux, or deposition temperature. Studies with silver films often reveal a clear tendency of Ag atoms to coagulate and form three-dimensional aggregates at a relatively early stage of growth instead of a plain layer-by-layer growth [58–61]. A current STM study of the Ag growth on a Re(0001) surface [62] reveals likewise a clear tendency of attractive Ag–Ag interactions.

For our specific system Ag/Ru(10$\bar{1}$0) the growth is largely dominated by the corrugation of the Ru substrate with its amplitude of almost 1 Å. A behavior of exactly this kind has been found with gold deposits on Ru(10$\bar{1}$0) [38,39], where about 15 Au layers were necessary to overcome the structural influence of the Ru substrate. In view of these findings it seems quite surprising that Kiskinova et al. [63] reported in their study of the Cu/Ru(10$\bar{1}$0) system pseudomorphic growth within the first Cu layer, followed by clear homoepitaxy already after deposition of three Cu layers. The reason why Cu (despite the fact that many of its thermodynamic properties such as heat of sublimation, surface free energy etc. resemble the respective Au data) behaves so differently is not known to us; it may be, however, that the somewhat smaller atomic radius of Cu ($r = 1.28$ Å, i.e., about 5% *smaller* than that of Ru) is decisive here in that it allows the filling of Ru surface troughs without any squeezing of the Cu atoms.

In conclusion, we underline the face-specificity in the heteroepitaxial growth of silver on ruthenium which leads to epitactic films with the characteristic bulk Ag lattice constant for deposition on the basal (0001) surface after deposition of only a few layers [53], while there is no such growth found up to eight Ag layers on the corrugated (10$\bar{1}$0) surface, where the film morphology is entirely determined by the substrate orientation.

Acknowledgements

We gratefully acknowledge financial support of this work by the Deutsche Forschungsgemeinschaft (through SFB 290) and the Fonds der Chemischen Industrie. We also thank K. Schubert and R. Cames for technical assistance.

References

[1] E. Bauer, Appl. Surf. Sci. 11/12 (1982) 479.
[2] E. Bauer, Ber. Bunsenges. Phys. Chem. 95 (1991) 1315, and references therein.
[3] E. Bauer, in: The Chemical Physics of Solid Surfaces and Heterogeneous Catalysis, Eds. D.A. King and D.P. Woodruff, Vol. 3 (Elsevier, Amsterdam, 1984).
[4] See, for example: P. Wissmann, Ed., Thin Metal Films and Gas Chemisorption, Studies in Surface Science and Catalysis, Vol. 32 (Elsevier, Amsterdam, 1987).
[5] V. Ponec, in: Catalyst Characterization Science, ACS Symp. Series 288, Eds. M.L. Deviney and J.L. Gland (American Chemical Society, Washington DC, 1985), p. 267, and references therein.
[6] V. Ponec, Adv. Catal. Rel. Subj. 32 (1983) 149.
[7] J.H. Sinfelt, Bimetallic Catalysts (Wiley, New York, 1983).
[8] J.H. Sinfelt, G.H. Via and F.W. Lytle, Catal. Rev. Sci. Eng. 26 (1984) 81.
[9] J.E. Houston, C.H.F. Peden, D.S. Blair and D.W. Goodman, Surf. Sci. 167 (1986) 427.
[10] J.A. Rodriguez, R.A. Campbell and D.W. Goodman, J. Chem. Phys. 95 (1991) 2477.
[11] J.W.A. Sachtler and G.A. Somorjai, J. Catal. 81 (1983) 77.

[12] J.W.A. Sachtler and G.A. Somorjai, J. Catal. 89 (1984) 35.
[13] C.T. Campbell, M.T. Paffett and A.F. Voter, J. Vac. Sci. Technol. A 4 (1986) 3055.
[14] M.T. Paffett, C.T. Campbell, T.N. Taylor and S. Srinivasan, Surf. Sci. 154 (1985) 284.
[15] D.E. Peebles, H.C. Peebles and J.M. White, Surf. Sci. 136 (1984) 463.
[16] J. Paul and F.M. Hoffmann, Surf. Sci. 172 (1986) 151.
[17] F.M. Hoffmann and J. Paul, J. Chem. Phys. 86 (1987) 2990; 87 (1987) 1857.
[18] C.T. Campbell, Annu. Rev. Phys. Chem. 41 (1990) 775.
[19] H. Shimizu, K. Christmann and G. Ertl, J. Catal. 61 (1980) 412.
[20] J.C. Vickerman, K. Christmann and G. Ertl, J. Catal. 71 (1981) 175.
[21] B. Sakkakini, A.J. Swift, J.C. Vickerman, C. Harendt and K. Christmann, J. Chem. Soc. Faraday Trans. I 83 (1987) 1975.
[22] E. Bauer, F. Bonczek, H. Poppa and G. Todd, Surf. Sci. 53 (1975) 87;
E. Bauer, H. Poppa, G. Todd and F. Bonczek, J. Appl. Phys. 45 (1974) 5164.
[23] J. Kolaczkiewicz and E. Bauer, Surf. Sci. 175 (1986) 508.
[24] M. Tikhov and E. Bauer, Surf. Sci. 203 (1988) 423.
[25] M. Mundschau, E. Bauer, W. Telieps and W. Swiech, Surf. Sci. 213 (1989) 381.
[26] J.T. Yates, C.H.F. Peden and D.W. Goodman, J. Catal. 94 (1985) 576.
[27] D.W. Goodman and C.H.F. Peden, J. Catal. 95 (1985) 321.
[28] C.H.F. Peden and D.W. Goodman, J. Catal. 100 (1986) 520.
[29] A. Brown and J.C. Vickerman, Surf. Sci. 140 (1984) 261.
[30] K. Christmann, G. Ertl and H. Shimizu, J. Catal. 61 (1980) 397.
[31] J.C. Vickerman, K. Christmann, G. Ertl, P. Heimann, F.J. Himpsel and D.E. Eastman, Surf. Sci. 134 (1983) 367.
[32] K. Wandelt, K. Markert, P. Dolle, A. Jablonski and J.W. Niemantsverdriet, Surf. Sci. 189 (1987) 114.
[33] J.W. Niemantsverdriet, P. Dolle, K. Markert and K. Wandelt, J. Vac. Sci. Technol. A 5 (1987) 114.
[34] Chr. Harendt, K. Christmann, W. Hirschwald and J.C. Vickerman, Surf. Sci. 165 (1986) 413.
[35] R.Q. Hwang, J. Schröder, C. Günther and R.J. Behm, Phys. Rev. Lett. 67 (1991) 3279.
[36] R.Q. Hwang, C. Günther, J. Schröder, S. Günther, E. Kopatzki and R.J. Behm, J. Vac. Sci. Technol. A 10 (1992) 1970.
[37] G. Pötschke, J. Schröder, C. Günther, R.Q. Hwang and R.J. Behm, Surf. Sci. 251/252 (1991) 592.
[38] Chr. Harendt, PhD Thesis, FU Berlin, 1987, and to be published.
[39] S. Poulston, M. Tikhov and R.M. Lambert, Surf. Sci. 331–333 (1995) 818.
[40] P. Lenz and K. Christmann, J. Catal. 139 (1993) 611.
[41] G. Lauth, T. Solomun, W. Hirschwald and K. Christmann, Surf. Sci. 210 (1989) 201.
[42] H. Conrad, H. Herz and J. Küppers, J. Phys. E 12 (1979) 369.
[43] D.W. Goodman and J.M. White, Surf. Sci. 90 (1979) 201.
[44] K. Harrison, R.M. Lambert and R.H. Prince, Surf. Sci. 176 (1986) 530.
[45] G. Lauth, E. Schwarz and K. Christmann, J. Chem. Phys. 91 (1989) 3729.
[46] D.A. King, Surf. Sci. 47 (1975) 384.
[47] J.P. Biberian and G.A. Somorjai, Appl. Surf. Sci. 2 (1979) 352.
[48] M.P. Seah and W.A. Dench, Surf. Interf. Anal. 1 (1979) 2.
[49] S. Tanuma, C.J. Powell and D.R. Penn, Surf. Interf. Anal. 11 (1988) 577.
[50] D. Kashchiev, J. Crystal Growth 40 (1977) 29.
[51] G.E. Rhead, M.G. Barthes and C. Argile, Thin Solid Films 82 (1981) 201.
[52] L. Pauling, Die Natur der chemischen Bindung, 2nd ed. (Verlag Chemie, Weinheim, 1964).
[53] B. Konrad, F.J. Himpsel, W. Steinmann and K. Wandelt, Proc. Int. Conf. ER-LEED, Erlangen, Germany (1985) p. 109.
[54] The heats of sublimation ΔH_{sub} simply were calculated by adding the heats of fusion ΔH_f and the heats of vaporization ΔH_v for the respective elements with the data taken from The Handbook of Chemistry and Physics, Chemical Rubber Company, 55th ed., Cleveland, Ohio, 1974/75.
[55] G. Ehrlich, Surf. Sci. 299/300 (1994) 628.
[56] J.A. Venables, Surf. Sci. 299/300 (1994) 798.
[57] See, for example: H.J. Güntherodt and R. Wiesendanger, Eds., Scanning Tunneling Microscopy I. 2nd ed. (Springer, Berlin, Heidelberg, New York, 1994).
[58] M.M. Dovek, C.A. Lang, J. Nogami and C.F. Quate, Phys. Rev. B 40 (1989) 11973.
[59] D. Winau, H. Itoh, A.K. Schmid and T. Ichinokawa, Surf. Sci. 303 (1994) 139.
[60] A.P. Sharpio, T. Miller and T.C. Chiang, Phys. Rev. B 37 (1988) 3996.
[61] H.C. Peebles, D.D. Beck, J.M. White and C.T. Campbell, Surf. Sci. 150 (1985) 120.
[62] M. Parschau, D. Schlatterbeck and K. Christman, Surf. Sci., submitted.
[63] M. Kiskinova, M. Tikhov and G. Bliznakov, Surf. Sci. 204 (1988) 35.